Mechanical Systems and Signal Processing 70-71 (2016) 958–973

Contents lists available at ScienceDirect

Mechanical Systems and Signal Processing

journal homepage: www.elsevier.com/locate/ymssp

General linear chirplet transform

Gang Yu *, Yiqi Zhou

Key Laboratory of High-Efficiency and Clean Mechanical Manufacture, Shandong University, Jinan 250061, PR China

ARTICLE INFO

Article history:
Received 28 April 2015
Received in revised form
24 August 2015
Accepted 1 September 2015
Available online 26 September 2015

Keywords:
Time–frequency analysis
Linear chirplet transform
Instantaneous frequency
Signal reconstruction

ABSTRACT

Time–frequency (TF) analysis (TFA) method is an effective tool to characterize the time-varying feature of a signal, which has drawn many attentions in a fairly long period. With the development of TFA, many advanced methods are proposed, which can provide more precise TF results. However, some restrictions are introduced inevitably. In this paper, we introduce a novel TFA method, termed as general linear chirplet transform (GLCT), which can overcome some limitations existed in current TFA methods. In numerical and experimental validations, by comparing with current TFA methods, some advantages of GLCT are demonstrated, which consist of well-characterizing the signal of multi-component with distinct non-linear features, being independent to the mathematical model and initial TFA method, allowing for the reconstruction of the interested component, and being non-sensitivity to noise.

1. Introduction

The signal processing technology as an important tool of understanding the physical world has attracted so much attentions in a fairly long period. Classical Fourier transform (FT) is a standard tool of revealing the overall frequency content by assuming the considered signal is stationary. However, the assumption of stationary cannot always hold in practice, and the concept of non-stationary is much closer to the reality, such as the vibration response of rotary machinery under non-stationary events (run-up, run-down speed, and even fault impacts), echolocation signals from bats, speech signals from human, etc. For non-stationary cases, overall frequency obtained from the FT is inadequate to describe these signals, and the concept of instantaneous frequency (IF) is more suitable for characterizing the time-varying features. The well-known definition of IF was proposed by Ville and it describes how fast a signal oscillates locally at a time instant [1]. The IF of a signal can be calculated from the derivative of the phase of its analytic signal, but it is just suitable for mono-component signal. Fortunately, time–frequency analysis (TFA) provides an alternative and powerful solution to characterize the IF features of non-stationary signals [2,3]. That is due to the energy distribution of time–frequency (TF) representation generated by TFA is concentrating at and around the IF of the analyzed signal in the TF plane. Then the IF of the signal under consideration can be estimated from the well-established TF representation. So in order to estimate the IF features precisely, the key point is that the TFA method can achieve a high TF resolution. There exist many types of TFA methods, and they can be generally separated into two categories: the linear TFA and the quadratic TFA. In classical linear TFA, such as short-time Fourier transform (STFT) and wavelet transform (WT), a signal is characterized by the inner product with a dictionary of atoms which have the TF location capability. So the TF resolution of the liner TFA is mainly determined by the TF atoms. According to the Heisenberg uncertainty principle, the liner TFA cannot achieve an arbitrarily high TF resolution at the same time. This is to say that a fine frequency resolution leads to a

* Corresponding author. Tel.: +86 531 88396551.
E-mail address: yugang2010@163.com (G. Yu).

http://dx.doi.org/10.1016/j.ymssp.2015.09.004
0888-3270/

coarse time resolution and vice versa. The conventional liner TFA is established on the assumption of the considered signal being piece-wisely stationary in a short time. This means that they essentially use horizontal lines to approximate the IF feature. However, for strongly modulated frequency signal, the IF of the signal is also time-varying in the short window, which will lead to a poor TF resolution [4,5]. In classical quadratic TFA, such as WVD, it is the FT of instantaneous autocorrelation function of a signal. The WVD can create a TF representation with high TF resolution for mono-component signal, but the cross-terms are inevitably introduced simultaneously when processing multi-component signal.

As seen from above analysis, conventional TFA methods are insufficient to provide a TF representation with high resolution due to their inherent restrictions. To improve the performance of TFA methods, many endeavors have been made for past many years, and plenty of effective methods are proposed. Generally, these methods can be divided into two strategies: TF reassignment and parameterized TFA.

TF reassignment method belongs to a post-processing technology, and it can improve the readability of TF representation obviously [6,7]. The reassignment operator aims to sharpen the TF representation by assigning the average of energy in a domain to the gravity center of these energy contributions. So the TF result after reassignment is much closer to the true IF of the signal. Recently, with the development of modern signal processing technology, Maes and Daubechies proposed a phase-based reassignment technique that they termed synchrosqueezing transform (SST), with additional advantage of allowing for straightforward extraction and reconstruction [8,9]. By the fundamental math formulation of reconstruction, the SST is more appealing than conventional reassignment methods with non-existence of reconstruction. SST has been applied in many fields successfully, such as analysis of ECG signals [10], micro-seismic signals [11], and rotating machine fault diagnosis, [12] etc. However, the strongly modulated frequency component and noise could destroy the original TF representation of the signal heavily. As a post-processing tool, these will damage the results of SST. This point has been recognized in many studies [12–14]. To overcome these drawbacks, several improved methods have been built. As indicated in Ref. [12], the SST is limited to reassign the frequency variable of TF representation but ignore the time variable, so SST just creates a good TF representation when processing purely harmonic signals. With this observation, Li [12,15] proposed a general SST by introducing a demodulated operator which can transform the time-varying frequency into constant frequency, and then the perfect TF representation could be obtained by SST. In order to process multi-component signals with different modulated frequencies, a generalized demodulation approach was employed [32], and an iterative general SST was proposed [16]. However a fact should be pointed out, in most practical cases, the modulated frequency of a signal cannot be known in advance. This means that we cannot obtain the precise demodulated operator for practical signals. So the practicality of the general SST will be discounted.

The parameterized TFA method is inspired by the fact that different analyzed window (such as different width and chirp rate) applied in STFT or CWT can achieve the different TF resolution. If we select the appropriate window function which can be consistent with the inherent characteristics of the considered signal, the obtained TF representation will have a much higher TF resolution. So the development of parameterized TFA is toward identifying the inherent features of the signal and constructing the window functions. The chirplet transform (CT) was designed by Refs. [17,18]. By using an extra parameter, chirp rate, the CT is able to create a well-concentrated TF representation for the linear modulated signal. Henry [19] proposed an adaptive TFA method by using maximum likelihood estimation to select the best width and chirp rate of analyzed window. Chassande-Mottin and Pai [20] developed an algorithm to search the best chirp rate according to the TF signature of a signal. Candes [21] proposed the chirplet path pursuit method to detect the highly oscillatory signals.

It can be seen that the early parameterized TFA methods utilize the piece-wisely linear window to approximate the time-varying TF features. However, when strongly non-linear signal encountered, it is not a good choice. In Ref. [14], Wang proposed a method called as matching demodulation transform (MDT). The MDT method utilized a time-variant demodulated operator to describe the non-linear IF features, which can enhance the energy concentration of TF representation obviously. In parallel, by introducing the rotation operator and shift operator in Ref. [22], it allows for constructing the non-linear window functions. If a non-linear model being consistent with the signal is used, the TF representation could be generated with better concentrated energy. Peng and his group have proposed several non-linear mathematical models to describe the inherent features of many types of the analyzed signals, such as polynomial model [22], spline model [23], and general warblet model [24]. They call these methods uniformly as general parameterized TFA (GPTFA) [25]. Although GPTFA shows a powerful ability to achieve the high TF resolution when analyzing the signal with strongly non-linear IF, its several limitations should not be neglected. Due to the complexity and diversity of practical cases, we cannot use an individual mathematical model to describe all types of the measured signals. Moreover, a well-established model is just suitable for the specified mono-component in the signal, so it cannot handle the signal of multi-component with different IF features. Furthermore, the parameterized model needs to be estimated from conventional TFA, so it is needed the initialized TFA with a fair energy concentration, or it will fail to estimate the precise model. With these restrictions, the GPTFA still has a wide space to improve.

As the recently advanced TFA technologies, SST and GPTFA can provide more precise insights into the complex structure of a signal, but their inherent limitations cannot be ignored. Considering their shortcomings, the improvement and development of TFA method should be directed at the following capabilities of (1) well-characterizing the multi-component signal with distinct non-linear features, (2) being independent to the mathematical model and initial TFA method, (3) allowing for the reconstruction of the interested component, (4) being as possible as non-sensitivity to noise. In this paper, we explore a new TFA method called as general linear chirplet transform (GLCT), which is able to achieve these goals as far as possible. With this prime objective, this paper is organized as follows. The theory of GLCT is described in Section 2 in detail. The numerical validation is carried out in Section 3. In Section 4, we give the detailed analysis about the property of GLCT. In Section 5, two bat signals and a vibration signal are utilized to illustrate the effectiveness of GLCT. The conclusion is given in Section 6.

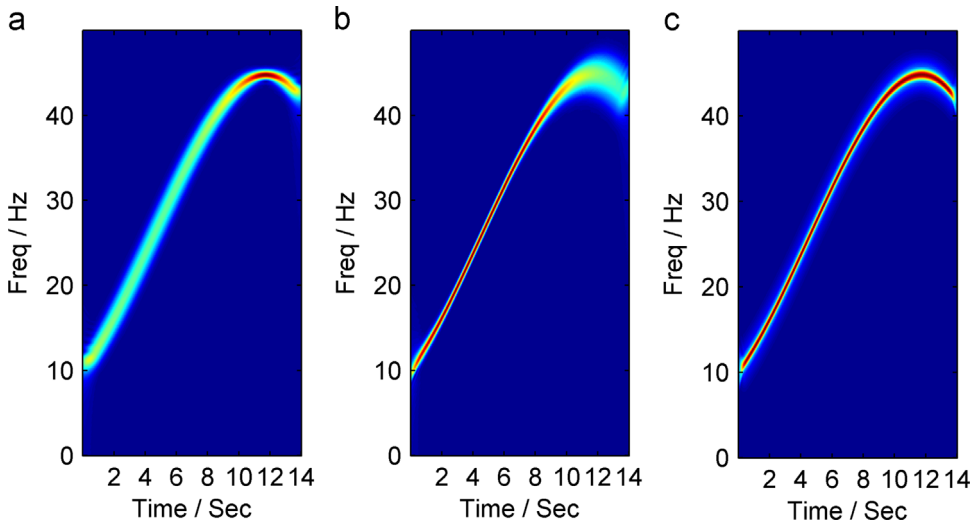

Fig. 1. TF representation by (a) STFT, (b) LCT, and (c) GLCT.

2. General linear chirplet transform (GLCT)

2.1. The motivation of GLCT

First of all, we use a numerical example to illustrate the motivation of our proposed method. This simulated signal is borrowed from Ref. [22] as follow:

$$s(t) = \sin(2\pi(10t + 5t^2/4 + t^3/9 + t^4/160)) \tag{1}$$

which is sampled at a sampling frequency of 100 Hz, and its IF is time-varying. The TF representations shown in Fig. 1(a) and (b), are generated by STFT and LCT (chirp rate $c = 4\pi$) respectively. Essentially, the STFT can be regarded as the LCT with chirp rate being zero. From the TF results in Fig. 1(a) and (b), it can be seen that, when the chirp rate of LCT is close to the true IF of the signal, the TF representation will have a high energy concentration. On the contrary, if the chirp rate of LCT is away from the true IF of the signal, the TF representation will smear heavily. As analyzed above, when the considered signal contains time-varying frequency component, it is impossible for any individual LCT to generate a TF representation with satisfactory energy concentration. Consequently, it is necessary to develop alternative methods to tackle this problem. An intuitive solution is motivated by combining the part with high energy concentration among the results generated by several LCT with different chirp rates. And the new TF representation will have better performance than any individual LCT, as shown in Fig. 1(c). Therefore, two problems to be solved arise. The first problem is how to determine the complete chirp rates of LCT, which make sure they can describe the time-varying frequency of a signal as precisely as possible. The second problem is how to determine the criterion which can select the appropriate TF representation generated by different LCT. In the following sections, we will give the solution for these two problems with detailed theoretical analysis.

2.2. The theory of GLCT

According to the theory of Ville, an analytic signal which considers time-varying IF can be written as

$$s(t) = A(t)\cdot e^{i\int \varphi(t)dt} \tag{2}$$

where $A(t)$ is the amplitude, and its IF can be written as

$$\mathrm{IF} = \varphi(t) \tag{3}$$

In a short time μ, the IF of signal $s(t)$ can be regarded as linear equation approximately, which can be expanded by Taylor expansion

$$\varphi(t)|_{t\in u} = \varphi(u) = \varphi(t') + \varphi'(t')(u - t') \tag{4}$$

where the reminder item is ignored, $\varphi(t')$ is the IF at time t', $\varphi'(t')$ is the first order derivative of IF at time t'.

Given a window $w(u-t')$ to truncate the signal, then FT of $w(u-t')\cdot s(u)$ in the IF $\varphi(t')$ can be calculated as

$$\begin{aligned}|S(\varphi(t'))| &= \left|\int_{-\infty}^{+\infty} w(u-t')\cdot s(u)\cdot e^{-i\varphi(t')u}du\right| \\ &= \left|\int_{-\infty}^{+\infty} w(u-t')\cdot A(u)\cdot e^{i\varphi(t')u+i\varphi'(t')(u-t')^2/2}\cdot e^{-i\varphi(t')u}du\right| \\ &= \left|\int_{-\infty}^{+\infty} e^{i\varphi'(t')(u-t')^2/2}\cdot w(u-t')\cdot A(u)\cdot e^{i\varphi(t')u}\cdot e^{-i\varphi(t')u}du\right| \\ &\le \left|\int_{-\infty}^{+\infty} w(u-t')\cdot A(u)\cdot e^{i\varphi(t')u}\cdot e^{-i\varphi(t')u}du\right| \\ &= \left|\int_{-\infty}^{+\infty} w(u-t')\cdot A(u)\cdot du\right| \end{aligned} \tag{5}$$

Eq. (5) denotes that, due to the presence of modulated element $e^{i\varphi'(t')(u-t')^2/2}$, the FT amplitude of $w(u-t')\cdot s(u)$ in its IF is lower than the harmonic component. Actually, the calculation by Eq. (5) is the STFT amplitude of the analytic signal in its IF. And this is the reason why the energy of TF representation of modulated part spreads out around the IF in a large area, but the energy of TF representation of harmonic part can concentrate on the IF with higher amplitude.

Given the standard STFT formulation as

$$S(t',\omega) = \int_{-\infty}^{+\infty} w(u-t')\cdot s(u)\cdot e^{-i\omega u}du \tag{6}$$

In order to eliminate the influence of modulated element, it is necessary to introduce a demodulated operator. Take into consideration that the linear modulated ratio $\varphi'(t')$ is a function of time, i.e. time-variant, the demodulated operator should be time-variant as well. Then the STFT of signal $s(t)$ which considers the time-variant demodulated operator, can be written as

$$S(t',\omega) = \int_{-\infty}^{+\infty} w(u-t')\cdot s(u)\cdot e^{-i\omega u}\cdot e^{-ic(t')(u-t')^2/2}du \tag{7}$$

For Eq. (7), the STFT amplitude of $s(t)$ in the IF $\varphi(t')$ which considers $e^{-ic(t')(u-t')^2/2}$ can be calculated by

$$\begin{aligned}|S(t',\varphi(t'))| &= \left|\int_{-\infty}^{+\infty} w(u-t')\cdot s(u)\cdot e^{-i\varphi(t')u}\cdot e^{-ic(t')(u-t')^2/2}du\right| \\ &= \left|\int_{-\infty}^{+\infty} w(u-t')\cdot A(u)\cdot e^{i\varphi(t')u+i\varphi'(t')(u-t')^2/2}\cdot e^{-i\varphi(t')u}\cdot e^{-ic(t')(u-t')^2/2}du\right| \\ &= \left|\int_{-\infty}^{+\infty} e^{i(\varphi'(t')-c(t'))(u-t')^2/2}\cdot w(u-t')\cdot A(u)du\right| \\ &\le \left|\int_{-\infty}^{+\infty} w(u-t')\cdot A(u)du\right| \end{aligned} \tag{8}$$

From Eq. (8), it can be seen that, if the demodulated operator is consistent with the modulated element of the analyzed signal, the STFT amplitude in the IF $\varphi(t')$ will achieve the maximum, and then the TF representation will concentrate on the IF with high energy concentration. Unfortunately, in most practical cases, the IF feature of a signal cannot be known in advance, which lead to that the demodulated operator $e^{-ic(t_\lambda)(u-t_\lambda)^2/2}$ is hard to be determined accurately, especially when multi-component existing. In this paper, we do not intend to identify the IF feature of the signal, and an alternative and easily-programmed method is proposed.

A feasible solution is to use a series of discrete demodulated operators to approximate the best demodulated operator $e^{-ic(t_\lambda)(u-t_\lambda)^2/2}$. Given the formulation of STFT which considers the discrete demodulated operator, as follows

$$S(t',\omega,c) = \int_{-\infty}^{+\infty} w(u-t')\cdot s(u)\cdot e^{-i\omega u}\cdot e^{-ic(u-t')^2/2}du \tag{9}$$

For each TF point (t',ω), if the discrete demodulated operator $e^{-ic(u-t')^2/2}$ is close to the modulated element of the signal, the TF representation around its IF will have high energy concentration and the amplitude $|S(t',\omega,c)|$ will reach the maximum among all values. Then for each TF point, according to the amplitude of $|S(t',\omega,c)|$, we can obtain the best argument c as

$$c' = \arg\max_c \left|S(t',\omega,c)\right| \tag{10}$$

and the TF representation of our proposed TFA method can be obtained as

$$GS(t',\omega) = S(t',\omega,c') \tag{11}$$

The spectrum can be defined as

$$\mathrm{Spec}(t', \omega) = |GS(t', \omega)|^2 \tag{12}$$

The next problem needed to be solved is how to determine the discrete demodulated operator $e^{-ic(u-t')^2/2}$. Actually, Eq. (9) is equal to the well-known linear chirplet transform, and this is the reason why our proposed method is called as general linear chirplet transform (GLCT). According to the research findings in Refs. [22,25], by introducing $e^{-ic(u-t')^2/2}$, it will produce a rotating effect on the TF result, and the rotating degree is $\arctan(-c)$. For a signal, if the sampling time (T_s) and sampling frequency (F_s) are determined, they will determine a TF plane $t \in (0, T_s)$, $f \in (0, F_s/2)$. So we can introduce a parameter α which can rotate in this TF plane, as

$$\alpha = \arctan\left(\frac{2T_s}{F_s}\cdot c\right), \quad \alpha \in (-\pi/2, \pi/2) \tag{13}$$

which make sure that the demodulated operator $e^{-ic(u-t')^2/2}$ can describe all feasible modulated element in the signal, then the Eq. (9) can be rewritten as

$$S(t', \omega, \alpha) = \int_{-\infty}^{+\infty} w(u-t')\cdot s(u)\cdot e^{-i\omega u}\cdot e^{-i\cdot \tan(\alpha)\cdot\frac{F_s}{2T_s}\cdot(u-t')^2/2}du \tag{14}$$

Suppose that the parameter α have N values, which can divide the TF plane into $N+1$ sections averagely, as

$$\alpha = -\pi/2 + \pi/(N+1), -\pi/2 + 2\cdot\pi/(N+1)\ldots -\pi/2 + N\cdot\pi/(N+1) \tag{15}$$

From above equations, it can be seen that, our proposed method just introduces one more parameter than STFT, i.e. N. If $N=1$, the GLCT will degenerate to be STFT.

We use a diagram to further illustrate the principle of GLCT ($N=3$) by comparing with STFT and LCT. In Fig. 2, the solid line denotes the true IF, dashed box denotes the analyzed window, and the gray area denotes the energy distribution of TF representation. In Fig. 2(a) and (b), due to the individual chirp window being used, if the demodulated ratio is close to the IF of the signal, the energy of TF representation will concentrate on the IF with a high TF resolution. However, if the demodulated ratio is significantly distinct with the IF of the signal, the energy of TF representation will spread out in a large area. In Fig. 2(c), by selecting the part with high energy concentration among the results generated by several LCT, the GLCT can achieve higher energy concentration around the IF than any individual LCT, so it can provide us with a more precise TF result.

3. Numerical validation

In this section, we use several numerical examples which consist of a mono-component signal and two multi-component signals to illustrate the performance of GLCT comparing with other TFA methods.

3.1. The mono-component signal

The first signal is considered as

$$s(t) = \sin(2\pi\cdot 25\cdot t + 2\pi\cdot 10\cdot \sin(t)) \tag{16}$$

whose IF is

$$\varphi(t) = 25 + 10\cdot\cos(t) \tag{17}$$

The results obtained by different TFA methods are shown in Fig. 3. As shown in Fig. 3(a), the energy of TF representation generated by WT spreads out around the IF, which results in a poor TF resolution. In Fig. 3(b), due to the presence of

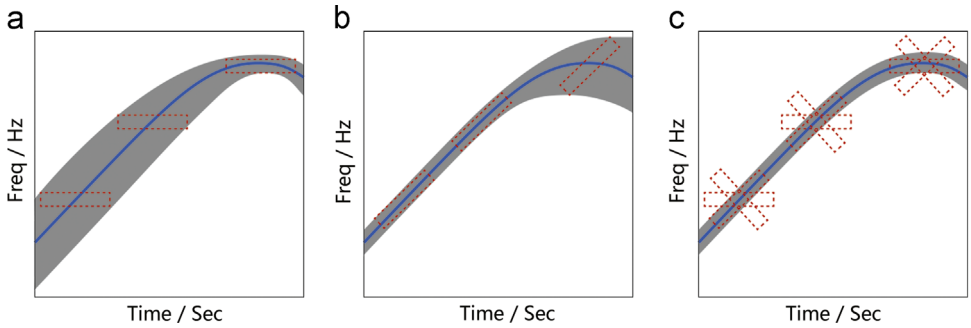

Fig. 2. TF energy distribution by (a) STFT, (b) LCT, and (c) GLCT.

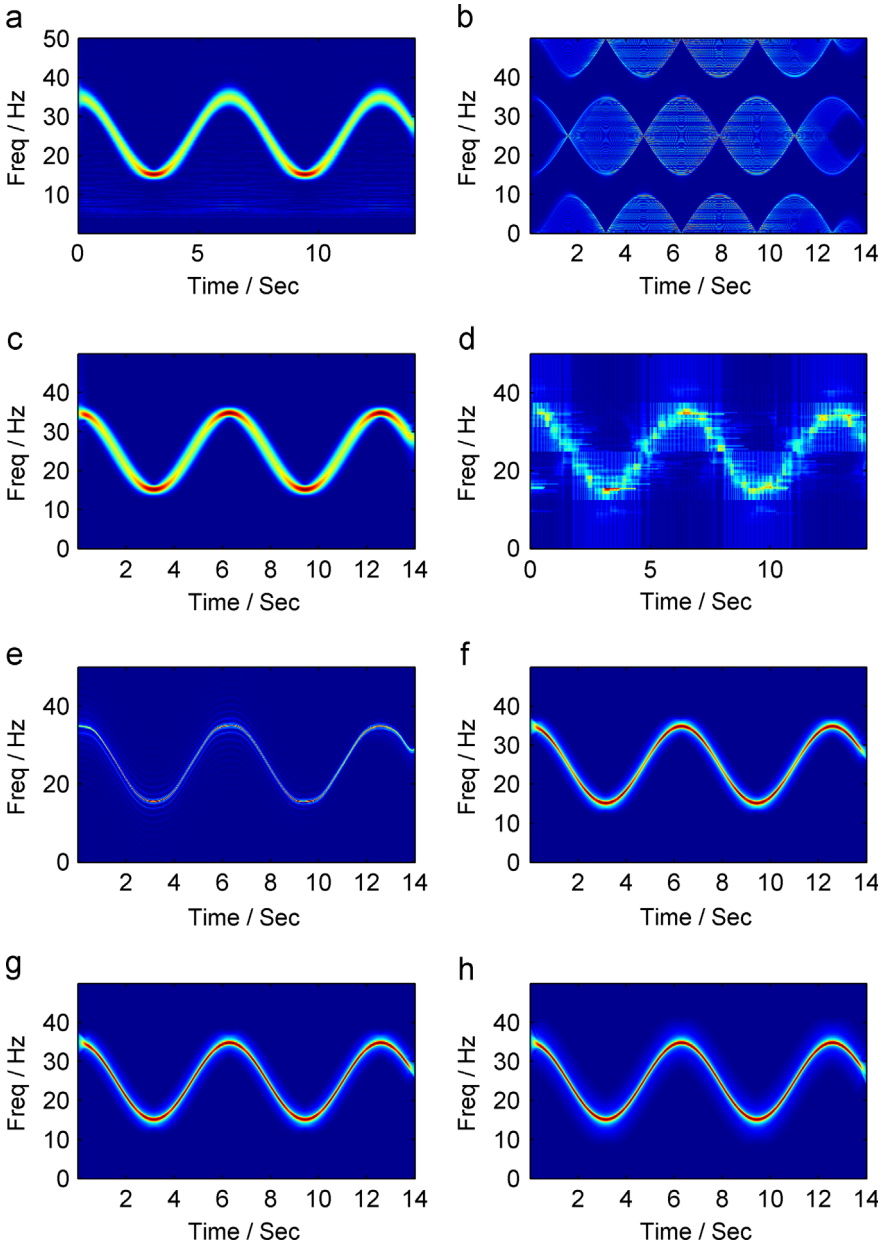

Fig. 3. TF representation by (a) WT, (b) WVD, (c) STFT, (d)AD, (e)SCT, (f) GLCT($N=5$), (g) GLCT($N=7$), and (h) GLCT($N=15$).

unexpected cross-term, the TF representation generated by WVD fails to give useful information about the signal. For the result of STFT shown in Fig. 3(c), the energy of TF representation is higher in the harmonic part than that in the modulated part. It can be seen that, due to the limitation of Heisenberg uncertainty, both the WT and STFT cannot achieve a high TF resolution in the time and frequency domain simultaneously, especially when analyzing the frequency-modulated signal.

The atomic decomposition (AD) method can achieve a sparse TF representation [30], but highly dependent on the selected atomic dictionary [31]. For the numerical signal, the 'Symmlet' is selected as the atomic function, and the TF result is shown in Fig. 3(d). It can be seen that, the selected atomic is not a good choice for non-stationary signal. Spline chirplet transform (SCT) is one special case of GPTFA [23], which is employed to analyze this signal. Firstly, it is needed to identify the IF feature based on original STFT, then construct the math model to characterize the signal in the TF plane, as shown in Fig. 3(e). The time-varying TF feature is characterized basically, while it needs extra procedure to estimate the IF.

For Fig. 3(f) (g) and (h), they are the results generated by GLCT with different parameters, i.e. $N=5$, 7 and 15 respectively, and the window length (WL) is set as 100 points. As can been shown that, with the increase of parameter N, the TF representation generated by GLCT have higher energy concentration, which is much closer to the ideal TF representation.

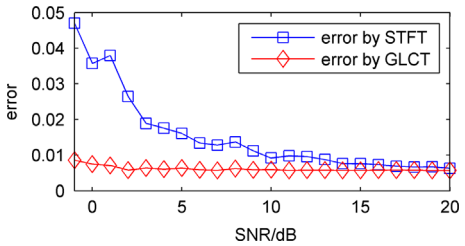

Fig. 4. The error of detected IF by STFT and GLCT.

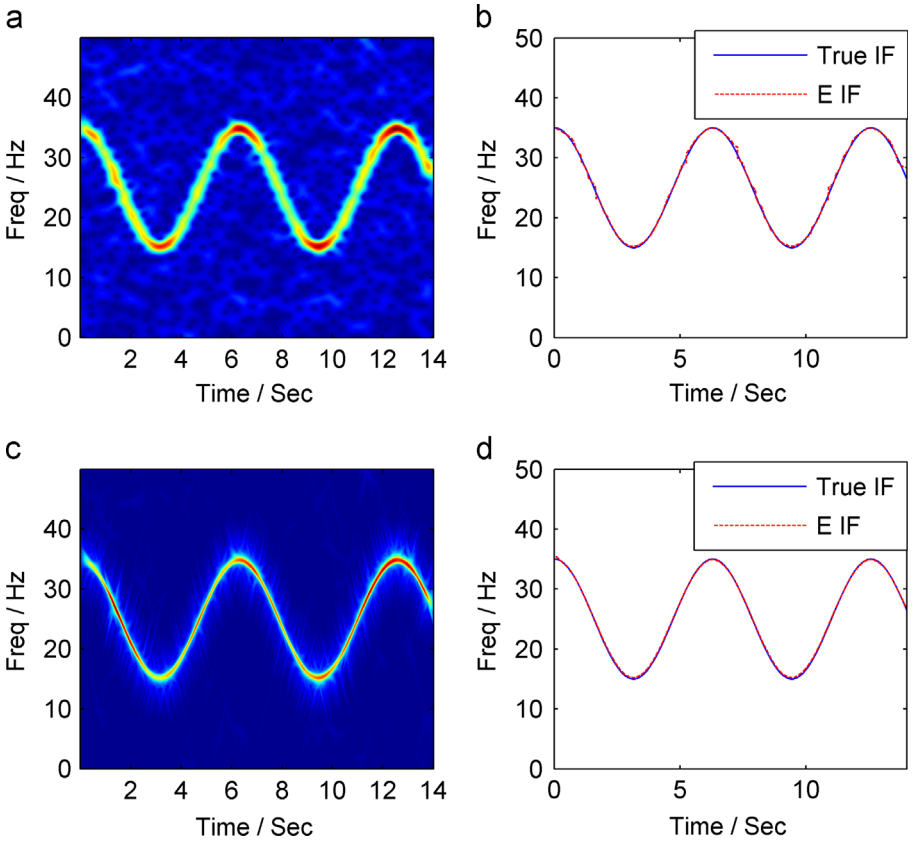

Fig. 5. SNR = 10 dB, (a) TF representation by STFT, (b) Detected IF, (c) TF representation by GLCT, (d) Detected IF.

Actually, when $N=7$ and 15, the TF representation generated by GLCT is satisfactory for charactering the true IF feature of the signal.

3.2. Estimation of IF feature

The IF of a signal is an important feature which can provide us with important information about the analyzed objective. In this subsection, we test the ability of GLCT detecting the IF feature of the signal to validate the performance of GLCT against noise. And the STFT is selected as the comparison reference. We add the noise with different SNR (signal to noise ratio) into the signal of Eq. (16). And the IF can be detected by the peak data from the TF representation. The detected error can be calculated by

$$\text{Error} = \text{mean}\left(\int \left| \frac{\text{IF}_e(t) - \text{IF}(t)}{\text{IF}(t)} \right| dt \right) \tag{18}$$

where $\text{IF}_e(t)$ denotes the estimated IF, $\text{IF}(t)$ is the true IF. Fig. 4 shows the calculated errors of estimated IF by two TFA methods. It can be seen that the IF estimated by GLCT ($N=7$ and WL = 100) is more robust against noise than by STFT. And to illustrate the detected procedure more clearly, we list the TF representation and the estimated IF under SNR = 10 dB and SNR = 0 dB. As shown in Fig. 5(a) and (b), when the noise of SNR = 10 dB is added, the IF detected by STFT is around the true IF, and the estimated error

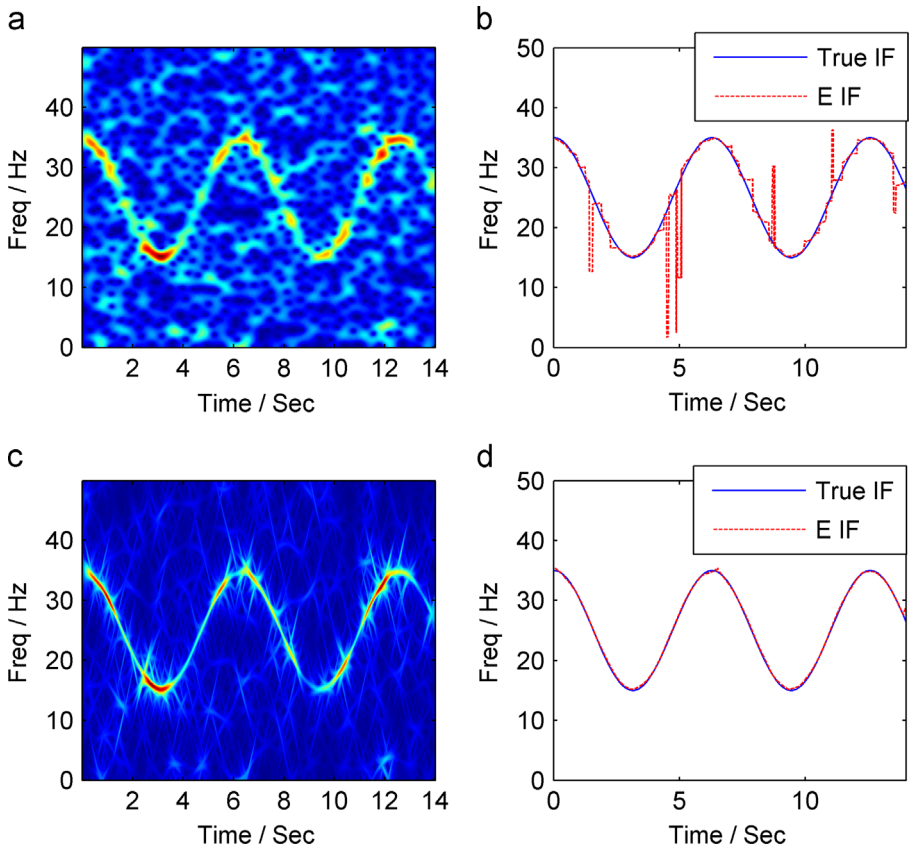

Fig. 6. SNR=0 dB, (a) TF representation by STFT, (b) Detected IF, (c) TF representation by GLCT, (d) Detected IF.

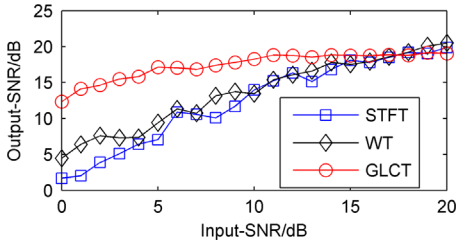

Fig. 7. The SNR of reconstructed signal by three methods.

is low. However, when the noise of SNR=0 dB is added, the IF detected by STFT occurs a large deviation with the true IF, especially in the modulated part, as shown in Fig. 6(a) and (b). This is due to that the amplitude of modulated part in signal is lower, which makes itself be affected more easily by noise than the harmonic part. The detected results of GLCT are shown in Figs. 5(c) and (d) and 6(c) and (d), when the noise of SNR=10 dB and SNR=0 dB are added, both of the estimated IF show satisfactory accuracy with the true IF.

3.3. *Signal reconstruction*

The prime objective of TFA can be formulated as the identification and reconstruction of interested components in a signal. So the reconstructed quantification is another significant indicator to evaluate the TFA method. For conventional methods, such as STFT and WT, there are two feasible types of reconstruction, direct reconstruction and ridge reconstruction. The reconstruction of direct method is to use the inverse formulation of TFA to extract the specified component by selecting the interested region in the TF representation, which is a widely applied method in most cases. However, the direct reconstruction method is not suitable for GLCT. The ridge reconstruction has been researched in many literatures, which denotes that the signal can be recovered using the TF representation data at the ridge points [26,27].

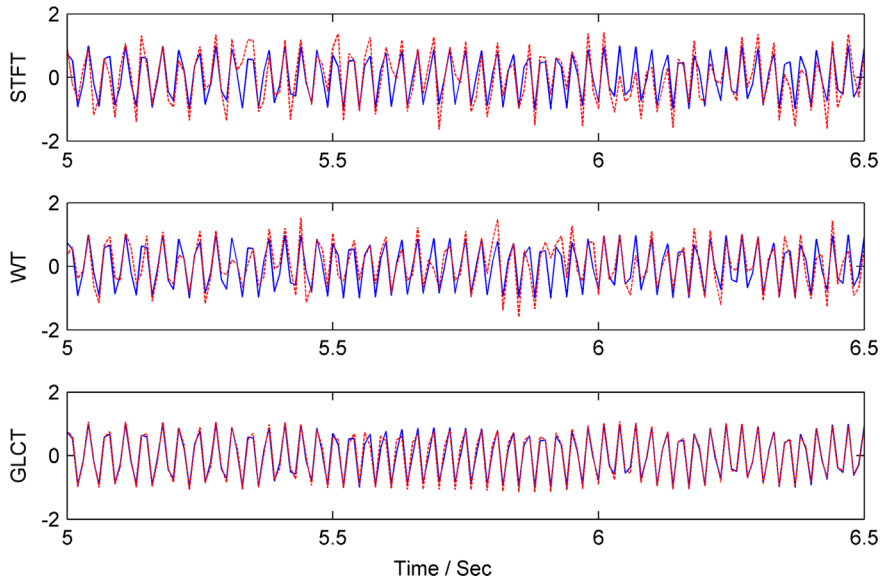

Fig. 8. The reconstructed signal at 5–6.5 s by STFT, WT and GLCT. (For interpretation of the references to color in this figure, the reader is referred to the web version of this article.)

For the TF representation of GLCT, when the ridge of interested component is estimated, the signal can be reconstructed by

$$s(t) = R(\mathrm{GS}(t, r(t)))/C_w \tag{19}$$

where $R(\cdot)$ denotes taking the real part, $\mathrm{GS}(t, \omega)$ is the TF representation of GLCT, and $r(t)$ is the detected ridge. $C_w = (1/2)\cdot\int_{-\infty}^{+\infty} w(t)dt$, $w(t)$ is the window function.

In this subsection, we test the ability of GLCT reconstructing the signal of Eq. (16) under different noise levels. For GLCT, we use the IF detected from peak data as the ridge parameter $r(t)$. We select the STFT and WT as the comparison reference, and the direct method is utilized to reconstruct the signal, which is evaluated by the SNR of reconstructed signals. The evaluated results are shown in Fig. 7. It can be seen that the GLCT has the best reconstructed ability in the low noise levels. For the noisy signal (SNR=0 dB), we list the reconstructed results at 5–6.5 s (see Fig. 8, the solid blue line is the original signal, the red dotted line denotes the reconstructed signal), which shows the GLCT provides the best reconstruction among the selected TFA methods. That is due to the added noise spreads out in the TF plane widely, so if the reconstructed region in TF plane is smaller, the noise introduced into the reconstructed signal will be less. The formulation of GLCT just considers the reconstructed region in the IF, so it should have the best reconstructed performance.

3.4. The multi-component signal

The second numerical signal with multi-component is considered as

$$\begin{cases} s_1(t) = \begin{cases} \sin(2\pi\cdot(33\cdot t + 10\cdot\sin(t))), & 0 < t \le 6 \\ \sin(2\pi\cdot 42.2\cdot t), & 6 < t \le 14 \end{cases} \\ s_2(t) = \begin{cases} \sin(2\pi\cdot(25\cdot t + 10\cdot\sin(t))), & 0 < t \le 6 \\ in(2\pi\cdot 34.2\cdot t), & 6 < t \le 14 \end{cases} \\ s_3(t) = \sin(2\pi(8\cdot t + 3\cdot\arctan((t-5)^2))), \quad 0 < t \le 14 \\ s(t) = s_1(t) + s_2(t) + s_3(t) \end{cases} \tag{20}$$

whose IF is plotted in Fig. 9(a). It can be seen that the components $s_1(t)$, $s_2(t)$ have the same modulated component but different initial frequency, and the $s_3(t)$ has distinct modulated component with others. To compare with other methods, we list the TF representation generated by different methods, such as WT, STFT, GPTFA, SST and GLCT (N=7 and WL=100).

The conventional liner TFA methods, STFT and CWT, are established on the assumption of the considered signal is piecewisely stationary in a short time. As shown in Fig. 9(b) and (c), when the IF of the signal is constant, the TF representation generated by WT and STFT can concentrate on the true IF with high energy concentration. However, for the modulated part, the energy of the TF representation spreads out in a large area around IF, which result in a low resolution. So the conventional methods are restricted to provide precise results for the signal with time-varying IF.

For GPTFA, by identifying the IF feature of a signal and constructing a non-linear demodulated operator, the TF representation can achieve a high TF resolution for the signal with IF feature being well-identified. However, for the component

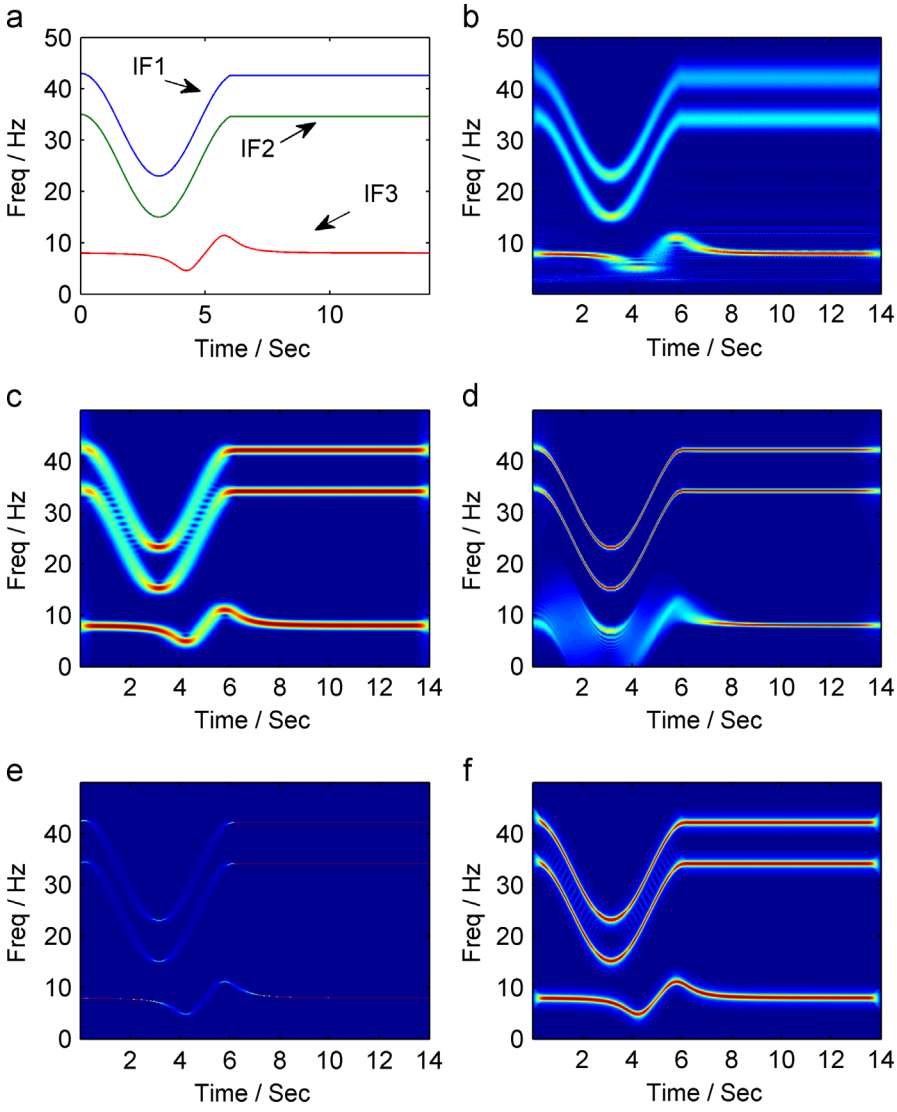

Fig. 9. (a) True IF, TF representation by (b) WT, (c) STFT, (d) GPTFA, (e) SST, and (f) GLCT.

with distinct IF features, due to the mismatch between the selected parameter and the component, GPTFA even may provide a poorer TF representation than STFT. For the TF result shown in Fig. 9(d), the mathematical model of $s_1(t)$, $s_2(t)$ is selected as the parameter of GPTFA, so these two signals can be characterized clearly. But the TF result of $s_3(t)$ shows a poor energy concentration. So GPTFA is limited to analyze the signal of multiple components with distinct IF features. Therefore, the main tasks of GPTFA focus on separating the signal of multi-component into multiple signals with mono-component, and constructing precise mathematical model to identify the IF feature of mono-component signal [28,29].

SST, as a post-processing TFA method, has to be restricted to the drawbacks of initial TFA methods. There exist two feasible SST solutions, SST based on WT and SST based on STFT. The result in Fig. 9(e) is generated by the latter method. It can be seen that, the harmonic part has the highest energy concentration among all TFA methods, however, the modulated part smear heavily. So in order to enhance the performance of SST, a feasible solution is to improve the result of the initial TFA method [14].

For the result in Fig. 9(f), the GLCT provides a satisfactory TF representation, which characterizes all components clearly. And the energy distribution is well-concentrated averagely on the true IF.

3.5. *The multi-component signal with crossed IF*

In Section 3.4, the numerical multiple components have the well-separated IF. However, it is necessary to consider the signal with crossed IF, which are often encountered in practice. Given three numerical sources as

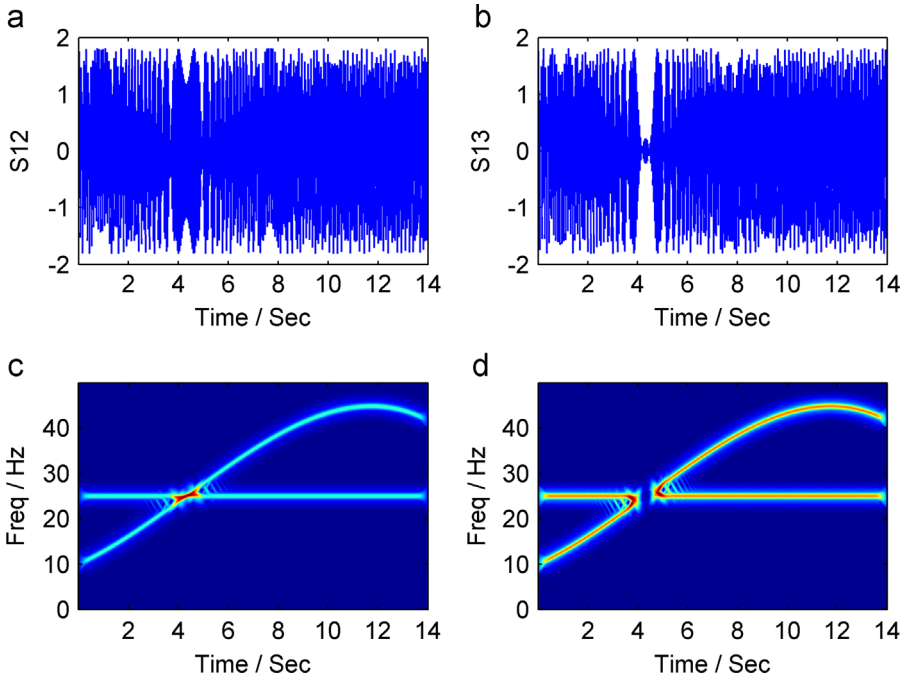

Fig. 10. The waveform of (a) S12 and (b) S13, the TF representation of (c) S12 and (d) S13.

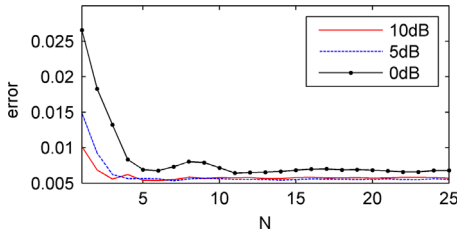

Fig. 11. The error of detected IF using different parameter *N*.

$$\begin{cases} s_1(t) = \sin(2\pi(10t + 5t^2/4 + t^3/9 + t^4/160)) \\ s_2(t) = \cos(2\pi \cdot 25t + 0.7\pi) \\ s_3(t) = \cos(2\pi \cdot 25t + 1.2\pi) \end{cases}$$

Actually, the component $s_1(t)$ is the signal of Eq. (1). The components $s_2(t)$ and $s_3(t)$ are the purely harmonic signal, which have the same frequency but distinct phases. Two multi-component signals are considered as $s_{12} = s_1 + s_2$ and $s_{13} = s_1 + s_3$ respectively. So in the TF plane, the signals s_{12} and s_{13} should have the same crossed TF point at (4.3 s and 25 Hz). To demonstrate the performance of GLCT more clearly, we list the waveform of s_{12} and s_{13} as shown in Fig. 10(a) and (b). It can be seen that, at the crossed time 4.3 s, the amplitude of s_{13} is lower than that of s_{12}. This is due to the superposition of s_1 and s_3 producing a decreased effect on the amplitude of s_{13}. While the superposition of s_1 and s_2 has an increased effect. Except for the crossed TF point, other points have the same amplitude. From the TF results by GLCT (see Fig. 10(c) and (d)) ($N=7$ and WL$=100$), they reflect this phenomenon clearly.

4. Selection of parameter

For GLCT, how to select the appropriate parameters such as *N*, window type, window length, is crucial to generate a good TF result. So it is necessary to analyze the impact of different parameters on the TF representation.

4.1. Selection of parameter N

From the numerical results in Fig. 3, it can be seen that, with larger *N* being selected, the TF representation has higher concentrated energy in the IF. So the estimation of IF can be achieved more accurately. In order to illustrate the effect of

Table 1
The cost time of different TFA methods.

TFA	WT	WVD	STFT	GLCT($N=5$)	GLCT($N=7$)	GLCT($N=15$)
Time (s)	1.56	0.73	0.81	4.61	6.05	14.21

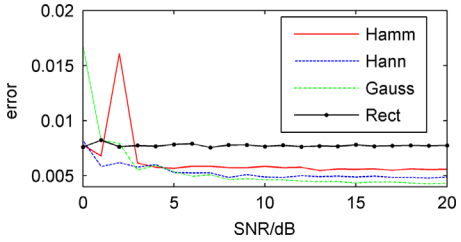

Fig. 12. The error of detected IF using different window functions.

parameter N clearly, we use the error of IF estimation to evaluate the performance of GLCT. The signal of Eq. (16) under different noise levels (10 dB, 5 dB, and 0 dB) is considered. The estimated results are listed in Fig. 11. It can be seen that, with increase of N, the error of IF estimation decreases. For $N > 11$, the error reduction is not obvious. However, the computational cost will increase.

The computational cost of GLCT mainly focuses on LCT (Eq. (9)) and maximum detection (Eq. (10)). Assuming that a signal of M samples is utilized, and the number of LCT is N, we obtain the computational complexity by the following procedure. Firstly, we compute the LCT with N times, so the computation is $O(NM^2 \log_2 M)$. Then we can obtain a $N \times M/2 \times M$ matrix. Secondly, we need to detect the maximum from this matrix with computation $O(NM^2)$. Therefore, the computational complexity of GLCT should be $O(NM^2 \log_2 M)$.

In following, we give the cost time of GLCT applied in analyzing the numerical signal of Eq. (16), comparing with other TFA methods. The tested computer is as follows, CPU: Intel Pentium 4 2.0 GHz, RAM: 1.0 GB. The cost times are listed in Table 1. It can be seen that, with the increase of parameter N, the cost time of GLCT increases obviously. So it is suggested to take a tradeoff between accuracy and efficiency.

4.2. Selection of window type

Selecting an appropriate window will be of benefit to the TF result, so it is required to determine the best optimal window. The popular windows include Hamming window, Hanning window, Gaussian window and rectangular window, etc. We take these four types of window to analyze the signal of Eq. (16) under different noise levels, and to evaluate the performance of GLCT. The error between peak data and IF is selected as the evaluation index, as shown in Fig. 12. It can be seen that, the Gaussian window has the best robustness against noise in the high SNR level, but shows a bad performance in the low SNR level. The Hanning window provides a better result of IF estimation in the low SNR level. So the Gaussian window is more suitable for the signal with high SNR, and the Hanning window is more suitable for the signal with low SNR.

4.3. Selection of window length

The GLCT is established on the linear TFA, so it is restricted to the uncertainty relationship between the time and frequency resolution. To obtain a high frequency resolution, we should use a long window. According to Eq. (4), we consider the IF in a short window with the one-order Taylor expansion, which denotes that the IF can be regarded as linearity approximately in a short time. However, in this short time, if the IF is strongly non-linear, the Taylor reminder will be large, which may lead to large error for this approximation. So for strongly non-linear IF, we need to select a short window to decrease the approximate error.

We utilize a numerical example to illustrate the effect of window length on the TF representation. We take the signal of Eq. (16) to analyze, and list the TF results by GLCT with different window length (WL=50, 120, 250 and 400 points, $N=7$ for all), as shown in Fig. 13. It can be seen that, when the window length is 50 points, the TF representation (see Fig. 13(a)) has a low frequency resolution. When the window length is increased, the frequency resolution is enhanced. But for window length being 400 points, due to the large approximate error for Taylor expansion, the TF result cannot provide a satisfactory TF result (see Fig. 13(d)). Therefore, it is suggested to take a tradeoff between frequency resolution and window length.

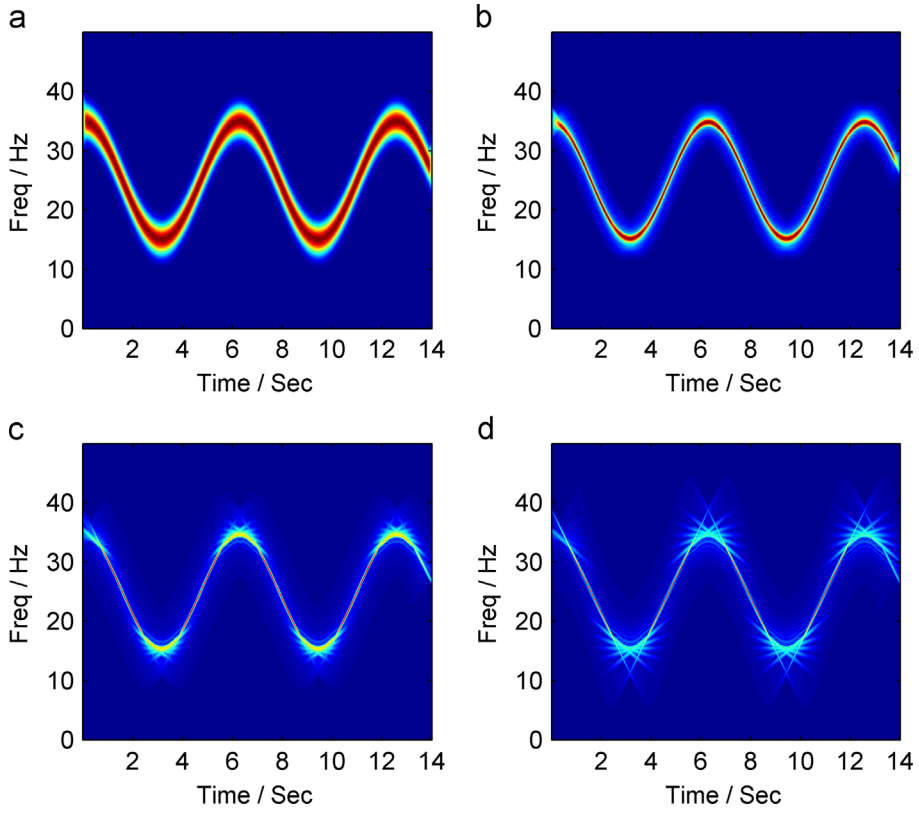

Fig. 13. The TF representation using different window length (a) 50, (b) 120, (c) 250 and (d) 400.

5. Experimental validation

5.1. Echolocation signals

In this subsection, we consider the application of GLCT in echolocation signal. By producing the frequency-modulated and sweeping-downward signal, and collecting the echo-delay signal, the bats can identify the object successfully in the complex environment. We use two groups of echolocation signals which consist of a mono-component signal and a multi-component signal to process, and select STFT as the comparison reference. The first signal is sampled at 1100 points and the TF representations (see Fig. 14(a) and (b)) are resulted from STFT and GLCT respectively. It can be seen that, STFT can generate the TF representation for the purely harmonic part (about 400–1000 points) with high energy concentration, but fails to characterize the TF features in the modulated part (about 100–400 points). The TF representation generated by GLCT ($N=15$, WL$=100$) provides us with an intuitive and clear result with higher energy concentration. The second signal is sampled at 400 points, and the TF representations in Fig. 14(c) and (d) are generated by STFT and GLCT ($N=31$, WL$=120$) separately. Similarly, the GLCT provides a superior TF result over STFT.

5.2. Vibration signal

The instantaneous rotating speed is an important indicator to evaluate the operating condition of rotary machinery, which is widely applied in condition monitoring, real time control, and fault diagnosis, etc. The direct measurement of rotating frequency (RF) is dependent on the extra hardware mounted on the shaft. However, it is usually costing or not easy, due to difficult installed conditions or shaft accessibility problems. To overcome this limitation, the estimation of RF by vibration signal has been a hot topic in engineering applications [22,33]. In this subsection, we focus on the application of GLCT in detecting the RF of rotary machinery under non-stationary condition.

The vibration signal is collected at a test rig (see Fig. 15) during a start-up about 500–2500 rpm (8.33–41.67 Hz) and a run-down about 2500–500 rpm. The test rig consists of a control cabinet, a drive motor, a test gearbox, a load gearbox and a load motor. Due to the main concern is the instantaneous speed, so we set the load being 0 N/m. An acceleration sensor is mounted on the test gearbox. Simultaneously, the rotating speed of shaft is measured by an inductive sensor (tacho-meter).

The vibration signal is recorded with a sampling rate of 5120 Hz and a sampling time of 113 s, as shown in Fig. 16(a), and the RF signal recorded by the inductive sensor is shown in Fig. 16(b). Considering the RF component is in the frequency range of 0–50 Hz, so we filter the signal in the band of 0–50 Hz, as shown in Fig. 17. The TF representation generated by GLCT ($N=7$, WL$=300$) is shown

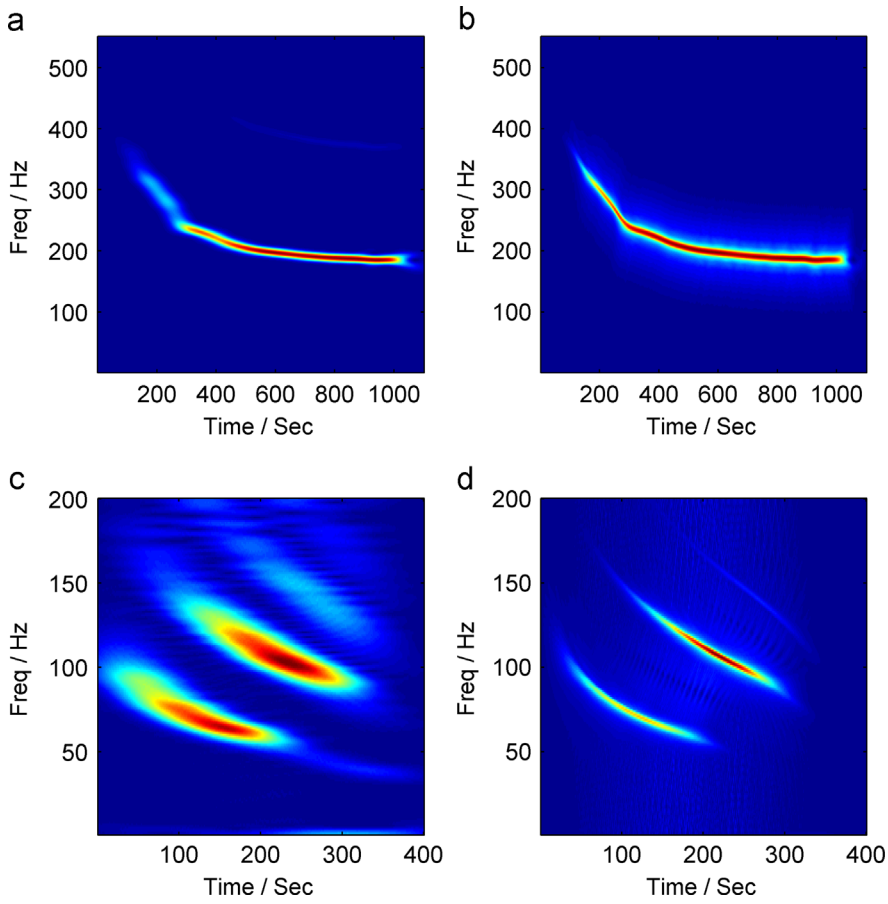

Fig. 14. TF representation of echolocation signals by (a) STFT, (b) GLCT, (c) STFT, and (d) GLCT.

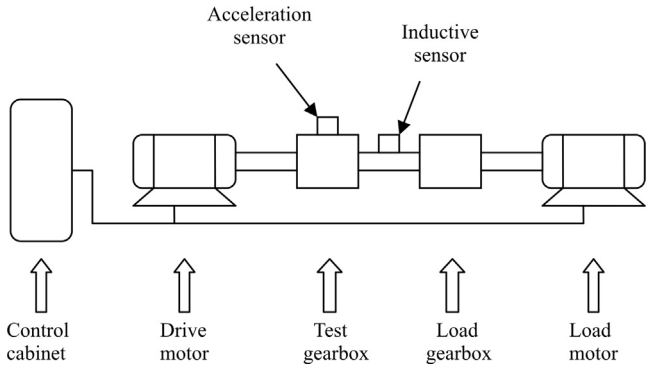

Fig. 15. The sketch of test rig.

in Fig. 18(a). It can be seen that, the RF component is characterized clearly in the TF plane, and the peak data of RF component is shown in Fig. 18(b). The IF of RF component provides us with an intuitive information that, the total speed-up consists of 22 local speed-ups, and the speed-down is a linearly reduction. From 500 to 2400 rpm (8.33–40 Hz), it needs 19 local speed-ups, and each speed-up is 100 rpm (1.67 Hz). In the last 3 local speed-ups, the speed of shaft increases from 2400 rpm to 2500 rpm. However, the RF measured by the inductive sensor cannot give us the detailed information like GLCT. Above analysis demonstrates that the change of instantaneous speed of shaft can be characterized precisely by GLCT, whose effectiveness is proved as well.

6. Conclusion

In this paper, we review the conventional and advanced TFA methods briefly, and point out their inherent limitations. By considering their limitations, we propose a new TFA method, called as GLCT, which can generate the TF representation with

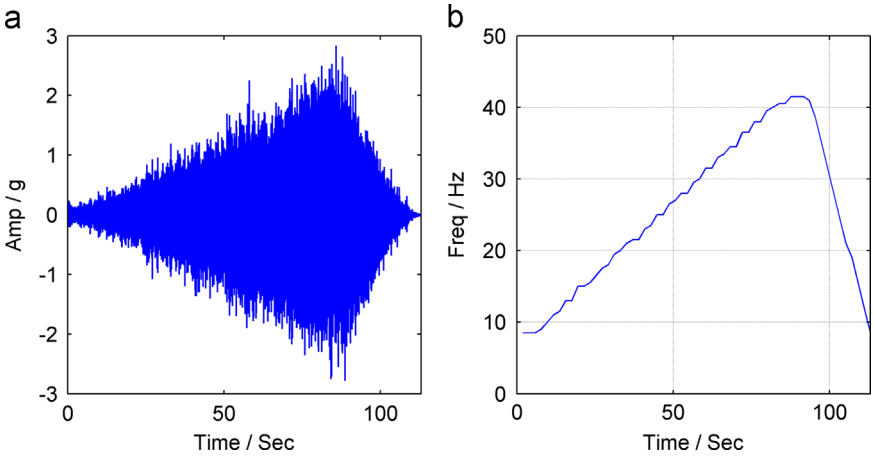

Fig. 16. (a) The waveform of recorded signal, and (b) the recorded RF by inductive sensor.

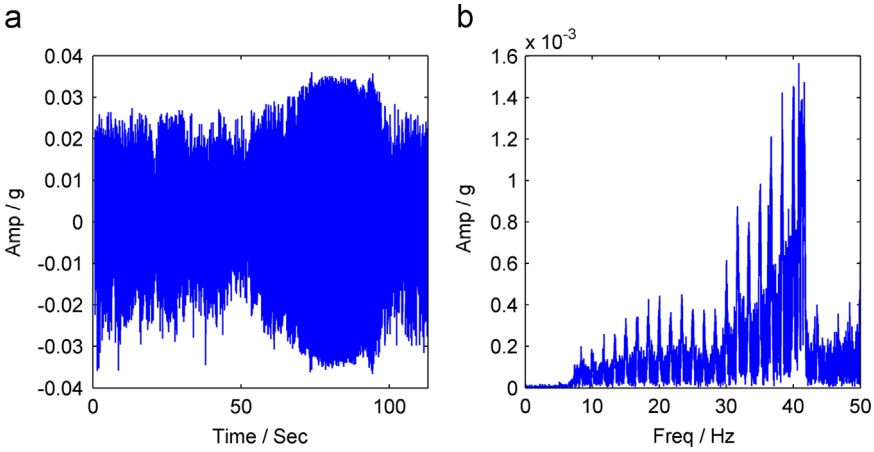

Fig. 17. (a) The waveform of filtered signal, and (b) its spectrum.

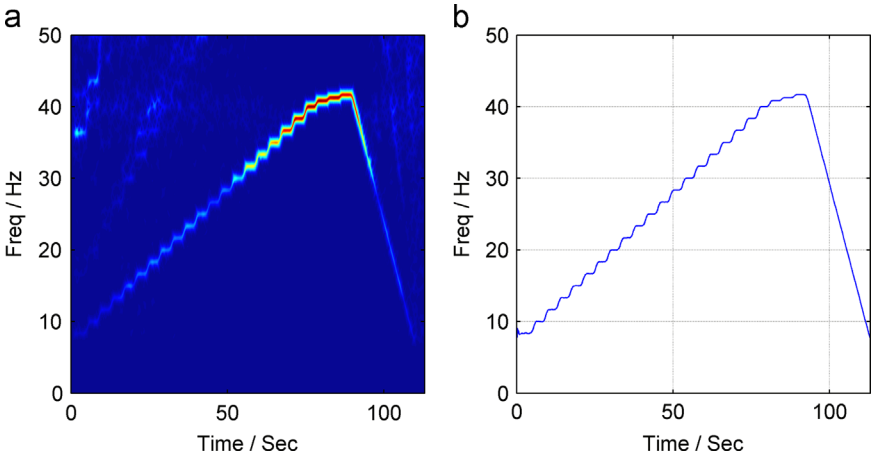

Fig. 18. (a) The TF representation and (b) the detected IF.

more satisfactory energy concentration and higher TF resolution. Compared with the conventional and advanced TFA methods, GLCT shows a superior ability to characterize the non-linear TF features accurately for both mono-component and multi-component signals. By estimating the IF of the signal and reconstructing the signal, the results indicate that GLCT is more robust against noise than conventional TFA methods. Two bat signals and a vibration signal are employed to demonstrate the effectiveness of our proposed method. In order to facilitate researchers' further study, we have published an original version of GLCT code on the web [34].

Acknowledgments

We are grateful to Peng Zhike for making his extended GPTFA technique available at: http://tfd.sourceforge.net/. And we wish to acknowledge D. Iatsenko for his SST code available at: http://www.physics.lancs.ac.uk/research/nbmphysics/diats/tfr/. This work was supported by the National Key Technology Research and Development Program 2015BAF07B04. We are grateful to the two anonymous reviewers for their valuable and detailed comments and suggestions which have helped to improve this paper.

References

[1] J. Ville, Theorie et application de la notion de signal analytic, Cables Transm. 93 (1948) 61–74.
[2] Cohen Leon, Time Frequency Analysis, Prentice Hall, Hunter College, , New York, 1995.
[3] S. Qian, D. Chen, Joint time–frequency analysis, Signal Process. Mag. IEEE 16 (1999) 52–67.
[4] J. Zhong, Y. Huang, Time–frequency representation based on an adaptive short-time Fourier transform, Signal Process. IEEE Trans. 58 (2010) 5118–5128.
[5] S.C. Pei, S.G. Huang, STFT with adaptive window width based on the chirp rate, Signal Process. IEEE Trans. 60 (2012) 4065–4080.
[6] F. Auger, P. Flandrin, Improving the readability of time–frequency and time-scale representations by the reassignment method, Signal Process. IEEE Trans. 43 (1995) 1068–1089.
[7] Z. Peng, F. Chu, Y. He, Vibration signal analysis and feature extraction based on reassigned wavelet scalogram, J. Sound Vib. 253 (2002) 1087–1100.
[8] I. Daubechies, S. Maes, A nonlinear squeezing of the continuous wavelet transform based on auditory nerve models, in: A. Aldroubi, M. Unser (Eds.), Wavelets in Medicine Biology, CRC Press, Boca Raton, 1996, pp. 527–546.
[9] I. Daubechies, J. Lu, H.T. Wu, Synchrosqueezed wavelet transforms: an empirical mode decomposition-like tool, Appl. Comput. Harmonic Anal. 30 (2011) 243–261.
[10] H.T. Wu, Y.H. Chan, Y.T. Lin, et al., Using synchrosqueezing transform to discover breathing dynamics from ECG signals, Appl. Comput. Harmonic Anal. 36 (2014) 354–359.
[11] P. Wang, J. Gao, Z. Wang, Time–frequency analysis of seismic data using synchrosqueezing transform, Geosci. Remote Sens. Lett. IEEE 11 (2014) 2042–2044.
[12] C. Li, M. Liang, Time–frequency signal analysis for gearbox fault diagnosis using a generalized synchrosqueezing transform, Mech. Syst. Signal Process. 26 (2012) 205–217.
[13] D. Iatsenko, P.V.E. McClintock, A. Stefanovska, Linear and synchrosqueezed time–frequency representations revisited, Digit. Signal Process. 42 (2015) 1–26.
[14] S. Wang, X. Chen, G. Cai, et al., Matching demodulation transform and synchrosqueezing in time–frequency analysis, Signal Process. IEEE Trans. 62 (2014) 69–84.
[15] C. Li, M. Liang, A generalized synchrosqueezing transform for enhancing signal time–frequency representation, Signal Process. 92 (2012) 2264–2274.
[16] Z. Feng, X. Chen, M. Liang, Iterative generalized synchrosqueezing transform for fault diagnosis of wind turbine planetary gearbox under nonstationary conditions, Mech. Syst. Signal Process. 52 (2015) 360–375.
[17] S. Mann, S. Haykin, The chirplet transform: physical considerations, Signal Process. IEEE Trans. 43 (1995) 2745–2761.
[18] S. Mann, S. Haykin, Adaptive chirplet transform: an adaptive generalization of the wavelet transform, Opt. Eng. 31 (1992) 1243–1256.
[19] H.K. Kwok, D.L. Jones, Improved instantaneous frequency estimation using an adaptive short-time Fourier transform, Signal Process. IEEE Trans. 48 (2000) 2964–2972.
[20] E. Chassande-Mottin, A. Pai, Best chirplet chain: Near-optimal detection of gravitational wave chirps, Phys. Rev. D: Part. Fields 73 (2006) 1–25.
[21] E.J. Candes, P.R. Charlton, H. Helgason, Detecting highly oscillatory signals by chirplet path pursuit, Appl. Comput. Harmonic Anal. 24 (2008) 14–40.
[22] Z.K. Peng, G. Meng, F.L. Chu, et al., Polynomial chirplet transform with application to instantaneous frequency estimation, Instrum. Meas. IEEE Trans. 60 (2011) 3222–3229.
[23] Y. Yang, Z.K. Peng, G. Meng, et al., Spline-kernelled chirplet transform for the analysis of signals with time-varying frequency and its application, Ind. Electron. IEEE Trans. 59 (2012) 1612–1621.
[24] Y. Yang, Z.K. Peng, G. Meng, et al., Characterize highly oscillating frequency modulation using generalized Warblet transform, Mech. Syst. Signal Process. 26 (2012) 128–140.
[25] Y. Yang, Z.K. Peng, X.J. Dong, et al., General parameterized time–frequency transform, Signal Process. IEEE Trans. 62 (2014) 2751–2764.
[26] R. Carmona, W.L. Hwang, B. Torrésani, Characterization of signals by the ridges of their wavelet transforms, Signal Process. IEEE Trans. 45 (1997) 2586–2590.
[27] R.A. Carmona, W.L. Hwang, B. Torresani, Multiridge detection and time–frequency reconstruction, Signal Process. IEEE Trans. 47 (1999) 480–492.
[28] Y. Yang, W. Zhang, Z. Peng, et al., Multicomponent signal analysis based on polynomial Chirplet transform, Ind. Electron. IEEE Trans. 60 (2013) 3948–3956.
[29] Y. Yang, X. Dong, W. Zhang, et al., Application of parameterized time–frequency analysis on multicomponent frequency modulated signals, Instrum. Meas. IEEE Trans. 63 (2014) 3169–3180.
[30] S.S. Chen, D.L. Donoho, M.A. Saunders, Atomic decomposition by basis pursuit, SIAM J. Sci. Comput. 20 (1998) 33–61.
[31] X. Wu, D. Yu, Atomic decomposition method based on adaptive chirplet dictionary, Adv. Adapt. Data Anal. 4 (2012) 1–19.
[32] S. Olhede, A.T. Walden, A generalized demodulation approach to time–frequency projections for multicomponent signals, Proc. R. Soc. A: Math. Phys. Eng. Sci. 461 (2005) 2159–2179.
[33] K.C. Gryllias, I.A. Antoniadis, Estimation of the instantaneous rotation speed using complex shifted Morlet wavelets, Mech. Syst. Signal Process. 38 (2013) 78–95.
[34] MATLAB Central File Exchange, 2015, File ID #50662. Available at: ⟨http://www.mathworks.com/matlabcentral/fileexchange/50662-general-linear-chirplet-transform⟩.